https://doi.org/10.1016/j.surfcoat.2016.11.052

Elsevier Editorial System(tm) for Surface and Coatings Technology

Manuscript Draft

Manuscript Number: SURFCOAT-D-16-01811R2

Title: Effects of Surface Nanocrystallization on The Corrosion Behaviors Of 316L And Alloy 690

Article Type: Full Length Article

Keywords: surface nanocrystallization, passive film, nitriding, corrosion resistance, nuclear plant materials

Corresponding Author: Ms. nana li,

Corresponding Author's Institution: Hong Kong Polytechnic University, Hong Kong, China

First Author: nana li

Order of Authors: nana li; sanqiang shi ; jingli luo, Prof; jian lu, prof; Ning Wang, Dr.

Abstract: Surface mechanical attrition treatments (SMATs) were used to prepare nanostructured surface layers on alloys used in nuclear power plant steam generators (SGs). The effects of surface nanocrystallization on alloy corrosion behavior at room temperature and at 300 °C in a simulated SG environment were studied. At room temperature, the polarization curves indicated that with increasing SMAT duration, the corrosion potential of the samples shifted negatively from smaller to larger values, and alloy active dissolution rate and passive current density both increased. Nitriding treatment was used to improve the corrosion resistance. Compared with corrosion behavior observed at room temperature, corrosion resistance in the simulated SG condition was highly enhanced because the nano-sized-grain layer formed via SMAT provided a higher density of nucleation sites for the formation of a passive film and diffusion paths for Cr, leading to the rapid formation of a dense protective oxide layer.

Dear editor,

I am Nana Li from The Hong Kong Polytechnic University. I am writing with regard to submit my paper to Surface Coatings &Technology. Please find the attached file. The title is " **Effects of Surface Nanocrystallization on The Corrosion Behaviors Of 316L And Alloy 690** ". Thanks for your attention.

Here is the contact information.
Corresponding author: Prof. Sanqiang Shi.
Telephone: 00852-27667821
Email: mmsqshi@polyu.edu.hk

With best regards
Nana Li

***Response to Reviewers**

Reviewer: 1	Comments to the Author	I sincerely apologize for the insufficient modification of last version as I had not got the new XPS results in time
1	In the new version, it is affirmed that the spectra were acquired with a step size of 0.1 eV, but looking the figure 5, the step size appears to be 0.2 eV, since I can see just 5 points in 1 eV. Therefore, the spectra have a low resolution and the peak-fitting analysis can't be considered corrected	The XPS test has been repeated and high-resolution spectra were taken at steps of 0.1 eV this time. The peak-fitting analysis has also been done with the same FWHM. The results were showed in Figure 5.
2	Moreover, the discussion is not sufficiently supported by the XPS results.	The XPS related analysis has been revised on page 11 line 3-11; page 10 line 12-13; page 12 line 2-6 and page 13 line 3-5

***Highlights (for review)**

High light:

- 316L after SMAT treatment show the poor corrosion resistance at the room temperature
- The corrosion resistance of SMATed 316L has been improved by nitriding treatment.
- SMATed alloy 690 exhibited superior corrosion resistance at a high temperature and high pressures.

https://doi.org/10.1016/j.surfcoat.2016.11.052

Effects of Surface Nanocrystallization on The Corrosion Behaviors Of 316L And Alloy 690

Nana Li[a,b], Sanqiang Shi[a,b*], Jingli Luo[c], Jian Lu[d], Ning Wang[e]

[a]The Hong Kong Polytechnic University, Shenzhen Research Institute, Shenzhen, 518057, China

[b]Department of Mechanical Engineering, the Hong Kong Polytechnic University, Hong Kong, China

[c]Department of Chemical and Materials Engineering, University of Alberta, Canada

[d]City University of Hong Kong, Hong Kong, China

[e]Southern University of Science and Technology, Shenzhen, 518055, China

Nana Li: Department of Mechanical Engineering, the Hong Kong Polytechnic University, Hong Kong, China

Email:nana.li@connect.polyu.hk; Tel:+852-55971880

Sanqiang Shi: Department of Mechanical Engineering, the Hong Kong Polytechnic University, Hong Kong,China

Email: mmsqshi@polyu.edu.hk;Tel: +852-27667821

Jingli Luo: Department of Chemical and Materials Engineering, University of Alberta, Canada

Email: jingli.luo@ualberta.ca;Tel: +780-4922232

Jian Lu: City University of Hong Kong, Hong Kong, China

Email: jianlu@cityu.edu.hk; Tel:+852-34426847

Ning Wang: Southern University of Science and Technology, Shenzhen, 518055, China

Email: wangn@mail.sustc.edu.cn; Tel: +86-75588018505

Corresponding author: San-Qiang Shi, Phone: +852-2766-7821.
E-mail address: mmsqshi@polyu.hk.

Abstract

Surface mechanical attrition treatments (SMATs) were used to prepare nanostructured surface layers on alloys used in nuclear power plant steam generators (SGs). The effects of surface nanocrystallization on alloy corrosion behavior at room temperature and at 300 $^{\circ}$C in a simulated SG environment were studied. At room temperature, the polarization curves indicated that with increasing SMAT duration, the corrosion potential of the samples shifted negatively from smaller to larger values, and alloy active dissolution rate and passive current density both increased. Nitriding treatment was used to improve the corrosion resistance. Compared with corrosion behavior observed at room temperature, corrosion resistance in the simulated SG condition was highly enhanced because the nano-sized-grain layer formed via SMAT provided a higher density of nucleation sites for the formation of a passive film and diffusion paths for Cr, leading to the rapid formation of a dense protective oxide layer.

Key Words *:* surface nanocrystallization, passive film, nitriding, corrosion resistance, nuclear plant materials

Corresponding author: San-Qiang Shi, Phone: +852-2766-7821.
E-mail address: mmsqshi@polyu.hk.

1. Introduction

Typical austenitic stainless steels 316L and the Ni-based alloy 690, have successfully been used in nuclear plants [1] as the main components both of structures supporting the nuclear core in the reactor pressure vessel and of pressurized boundary piping in pressurized water reactor (PWR) primary circuits. The aqueous environment in PWRs is subjected to high temperatures, pressures and irradiation levels. In this intense environment, most material failures occur on the surface; such failures include fatigue fracture, fretting fatigue, wear and corrosion. Thus, optimizing surface microstructures and properties may effectively enhance the global behavior of materials, particularly the service lifetime. Surface nanocrystallization (SNC) obviously improves the mechanical properties of metallic materials and has thus become an intensive research interest [2]. The surface mechanical properties of treated metallic substrates can be markedly enhanced by a single SNC treatment or by SNC combined with a thermal diffusion processes, such as nitriding [2-4], chromizing [5], and aluminizing. One of the most commonly used SNC methods is the surface mechanical attrition treatment (SMAT) [3]. This technique has been successfully applied in a variety of materials, including pure metals, steels, alloys, and intermetallics [6-10].

The SNC of such austenite stainless steels as 304,316L, and 321 has been well studied [7,11-13]. Zhang et al. studied the grain refinement mechanism of 304 and suggested that the formation of nanocrystallites in the top surface layer may be attributed to the much larger strain and strain rate [12]. SMAT is also effective for improving the tribocorrosion

behavior of 304 stainless steel in NaCl solution, in terms of reduced mechanical and chemical wear [14]. The mechanisms involved in the surface smoothening of 316L during SMAT have been elucidated by Arifvianto et al. [15]. Neverless, the SMAT process leads to residual stress with significant maximum stresses at the surface, which degrade the corrosion resistance of the materials in PWRs. Nitriding technique is of great industrial interest as the formation of a nitride layer in or on a ferritic surface layer leads to the improvement of material properties of the surface such as wear, fatigue, and corrosion resistance. [16]; nitriding treatment could improve both the strength and corrosion resistance of the treated sample. The mechanical properties of treated samples have been extensively investigated in previous studies. However, few reports have examined the electrochemical properties, which have important effects on corrosion, of treated samples with nitriding, especially under conditions of high pressure and temperature.

Compared with 316L, the oxide films formed on Ni-based alloys are believed to be important to their performance in PWRs. Carrette et al. [17] characterized the oxide film formed on alloy 690 in simulated PWR primary water and revealed that the film featured an Ni-enriched outer layer, a Cr-enriched inner layer, and an Ni-enriched interface between the oxide film and the alloy substrate. The work of Machet et al. [18] showed an outer Fe-rich layer on an inner Cr-rich layer in oxide films on nickel-based alloys in simulated PWR primary water. Ziemniak and Hanson [19,20] reported that oxide films formed on nickel-based alloys in hydrogenated, high-temperature water consisted of two layers of spinel: an Fe-rich outer layer and a Cr-rich inner layer. Sennour et al. [21] characterized the microstructure of oxide films formed on nickel-based alloys in simulated PWR primary

water and found that nodules of Cr_2O_3 were dispersed at the alloy/oxide interface and the external layer consisted of nickel ferrite. However, little is known about the structure or corrosion behavior of oxide films on treated 690 under high temperatures and pressures.

To fill the knowledge gap, this study investigated the influence of the nitriding process on the electrochemical behavior of treated 316L and the corrosion behavior of treated alloy 690 under high temperature and high pressure. X-ray photoelectron spectroscopy (XPS) was used to study the chemical composition and chemical state of the resulting oxide film on the metal surfaces under high temperature and pressure.

2. Experimental Materials and Methods

The commercially available stainless steel alloys 316L and alloy 690 were used for the experiments. The typical chemical compositions (mass percent, %) of the alloys are listed in Table 1.

Table 1. Chemical composition of the experimental materials (wt. %)

Type	C max	Mn max	P max	C max	Si max	Cr	Ni	Mo	Fe
316L	0.08	2.0	0.045	0.03	1.0	16-18	10-14	2-3	Bal
690	0.03	0.18	--	--	0.03	29.4	Bal	0.01	9.2

The different types of materials were ground/spark cut to be 1 mm ~ 2 mm in thickness. Then, they were degreased using acetone and subjected to SMAT using φ 3 mm 316L stainless steel balls for 15, 30, 45 and 60 mins at a fixed frequency of 20 kHz. SMAT was performed at room temperature. The SMAT details have been previously described [9]. Nitriding of the treated 316L were performed in a flowing NH_3 (99.9995%) at a total pressure of 1 atm. The phase transformation and residual stress were measured using

Philips, X-Pert X-ray diffraction (XRD) system. The instrument worked at a voltage of 40 KV and a current of 30 KA, with Cu Kα radiation. The scanning range was between 20°~110°, with the scan step size of 0.02°/s. The electrochemical behavior of untreated and treated alloys was evaluated by potentiodynamic polarization studies using well-established procedures that have been described elsewhere [9]. Potentiodynamic polarization measurements were carried out in the potential range from -100 mV to 120 mV at a scan rate of 100 mV/min in 3.5 wt. % NaCl solutions at room temperature. Prior to XPS and secondary ion mass spectrometry (SIMS), alloy 690 were pre-passivated in the test solution at 300 °C in an autoclave for 24 h. The chemical composition of the resulting passive film of alloy 690 was studied using XPS; these measurements were performed with an Axis-ULTRA (Kratos Analytical) spectrometer. Photoelectron emission was excited by an aluminum (monochromatized) source operated at 210 W with initial photon energy of 1486.71 eV. The survey spectra were recorded at steps of 0.33 eV using 160 eV pass energy, whereas high-resolution spectra were taken at steps of 0.1 eV using 20 eV pass energy. The base pressure was approximately 5×10^{-10} Torr. The C1s peak from adventitious carbon at 284.6 eV was used as a reference to correct the charging shifts. The photoelectrons were collected at a take-off angle of 90° with respect to the sample surface. The samples were cleaned using distilled water before the test. The concentration depth profile of the elemental distribution in the passive film was also investigated by a TOF-SIMS IV instrument (ION-ToF Gmbh). In the current work, Ga+ was used as the analysis source, operated at 15 kV; the sputtering source was Cs+, operated at 2 kV. To minimize atmospheric exposure, the samples were stored under argon until the SIMS test.

3. Results and Discussion

Figure. 1 (a) and (b) shows the XRD profiles of the treated 316L and 690 respectively. It can be seen from Figure 1(a) the untreated sample consisted of complete austenite (i.e., a face-centered cubic (fcc) structure with a lattice parameter of 0.361 nm). Bragg-diffraction peak broadening was induced in the four 316 steel samples treated for different durations; this result may be attributed to grain refinement and/or increased atomic-level lattice strain [22]. The XRD results showed that the surface layer of these samples remained mainly composed of single austenite, and no obvious phase transition was observed; the amount of the martensitic phase is negligible in comparison with the austenite phase under these SMAT conditions.

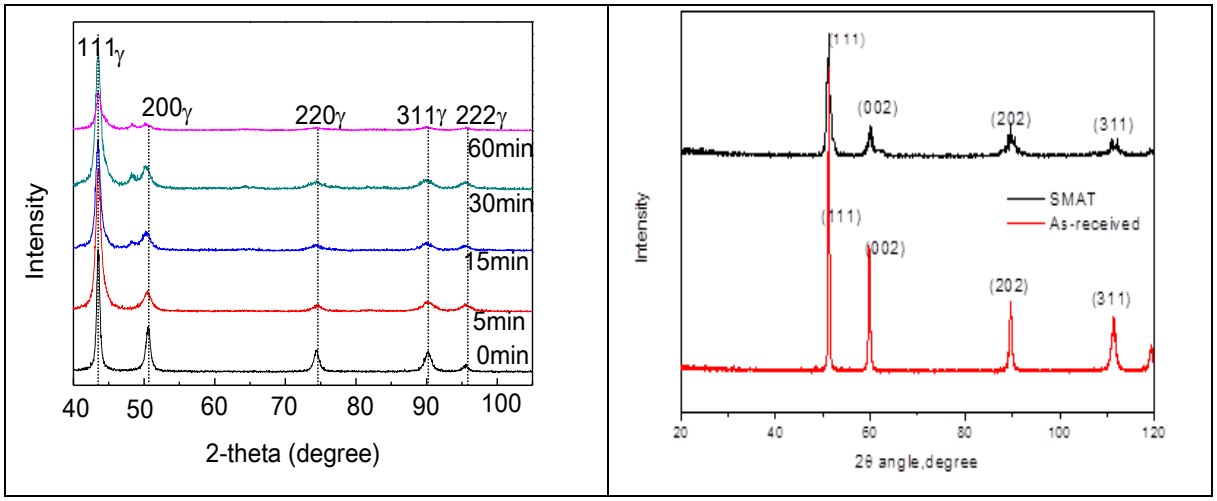

Figure 1. XRD profiles of (a) the untreated and treated 316 samples and (b) the untreated and treated 690 samples with different durations

The average grain size and mean microstrain of the treated 316L were calculated in terms of the diffraction line broadening of the five fcc-Fe Bragg reflection peaks (111), (200),

(220), (311) and (222) using the Scherrer and Wilson equation [23]. The results are listed in Table 2.

Table 2. Average grain size and mean microstrain in the surface layer of the 316L samples derived from XRD analysis

SMAT processing duration (min)	*D* (nm)	ε_2 (%)
5	21	0.182
15	17	0.201
30	13	0.228
60	9	0.263

The XRD peak broadening became less evident with increasing depth, indicating that grain size gradually increases and/or that microstrain decreases. The XRD profile of alloy 690 with different SMAT durations is similar to that on the 316L.

The potentiodynamic polarization curves at room temperature as a function of treatment time for 316L and 690 are separately shown in Figure. 2(a) and (b). All 316L samples exhibited typical passivation characteristics, and the corrosion potential of four samples shifted negatively at all treatment times.

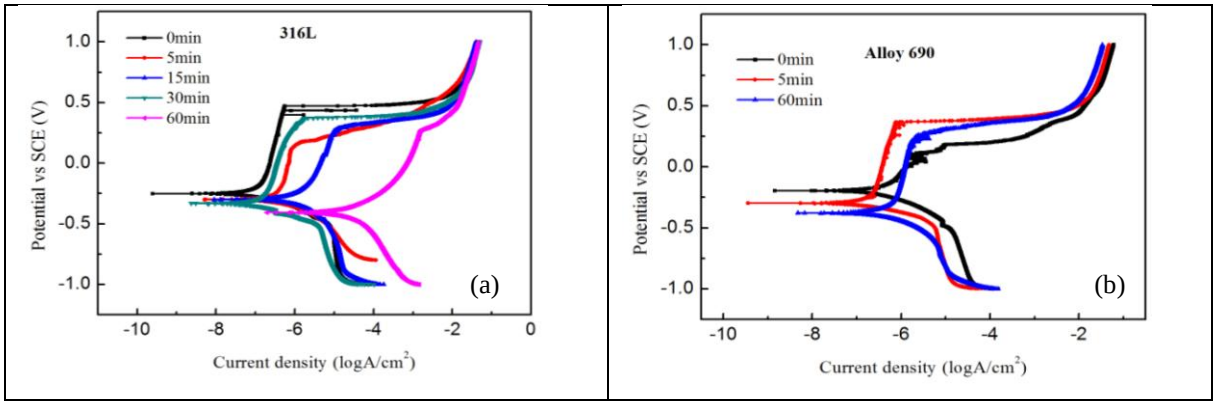

Figure. 2 Potentiostatic polarization curves of (a) 316L, and (b) 690 with different SMAT durations

The passive regions were relatively stable from 5 to 30 minutes. However, at 60 minutes, corrosion current density (I_{corr}) increased by one order of magnitude for 316L samples, indicating an obvious degradation of corrosion resistance; the I_{corr} of alloy 690 remained approximately the same as its value at 0 and 5 minutes of SMAT, indicating that SMAT exerts a very small effect on the corrosion properties of alloy 690 at room temperature.

Corrosion resistance became worse after SMAT treated on 316L due to reduced grain size and increased grain boundary density. In an attempt to release the high strain energy stored in the treated layer, we subjected the treated 316 steel to a nitriding treatment at 400°C for 6 h. The resulting polarization curve is shown in Figure 3. While the corrosion resistance of the nitriding processed 316L appeared to be superior to that of the treated sample, its corrosion potential was still lower than that of the untreated sample. It is possible that treated nanostructure recovery occurs after nitriding treatment.

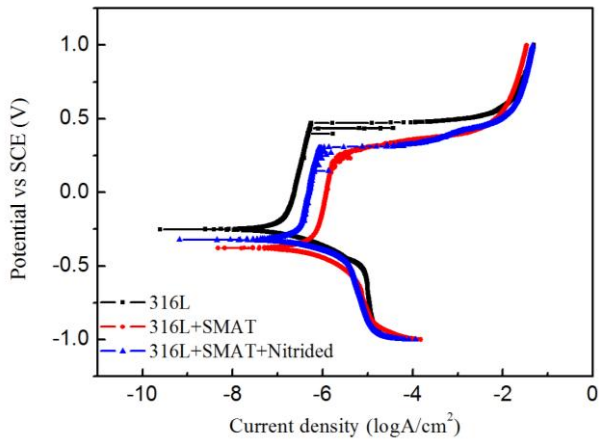

Figure.3 Treated 316L with nitriding treatment after SMAT.

To simulate the real conditions in SGs, potential dynamic measurements of alloy 690 were conducted in an autoclave at 300 °C, the results are shown in Figure. 4. All the samples showed an active-passive behavior in the corrosion solution under the applied potential. However, the treated samples exhibited excellent passivation ability. The breakdown potentials of the treated samples (5 min and 60 min) were more positive than that of the untreated sample, indicating that the nanocrystallized surface increases the passivation ability of alloy 690 at a high temperature. Moreover, alloy 690 exhibited a lower passive current density with 60 minutes of SMAT, indicating that a higher fraction of effective passive layer was produced at 300 °C.

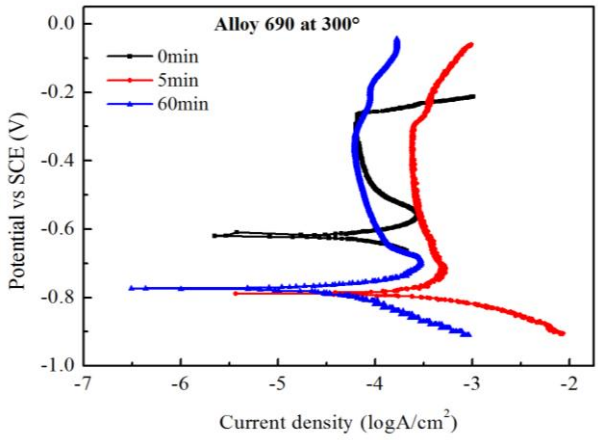

Figure 4. Polarization curves of alloy 690 at 300 °C after different SMAT durations.

To demonstrate the positive effect of SMAT on corrosion properties at a high temperature, passivation tests were carried out in the same autoclave, and the properties of the passive films were studied using XPS and SIMS Figure 5 showed the Cr $2p_{3/2}$ core level spectra of XPS and the Cr $2p_{3/2}$ peaks were systematically decomposed into two components for the 0 min,5 minutes and 60 minutes treatment; one component was located at a binding energy

(BE) of 576±0.5 eV, and another was located at BEs of 577.2 ± 0.1 eV. By comparison with published data [24-28], the signal at 576 eV can be attributed to Cr^{3+} in Cr_2O_3 [24,27,28], and the signal at 577.1 eV can be assigned to Cr^{3+} in $Cr(OH)_3$ [24,27]. From Figure5, it can be seen that the intensity of the signal of Cr_2O_3 remarkably increased and $Cr(OH)_3$ decreased with increasing SMAT time, which indicates that SMAT leads to a significant increase in the amount of Cr oxide in the passive film. This *a*-Cr_2O_3 has been reported [29] to be the stable crystalline form of chromium oxide, which can passivate the surface of a series of nickel alloys in the steady state at high temperature.

The anodic reactions of $Cr(OH)_3$ into Cr_2O_3 can be expressed as the following:

$$Cr^{3+}+3OH^- \rightarrow Cr(OH)_3 \qquad \text{(Eq.1)}$$

$$Cr(OH)_3+Cr \rightarrow Cr_2O_3+3H+3e^- \qquad \text{(Eq.2)}$$

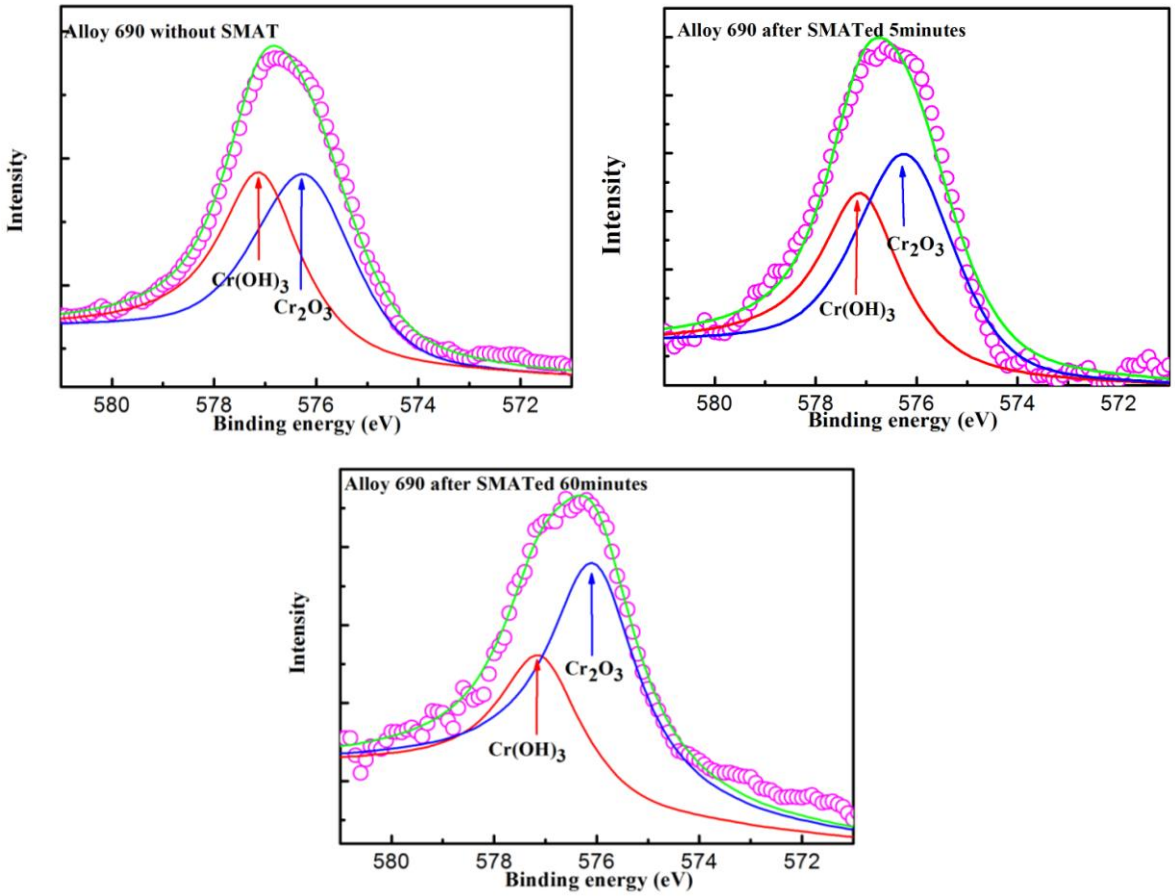

Figure. 5. Cr $2p_{3/2}$ core-level spectra of alloys 690 after treated for 0,5 and 60 minutes respectively exposed to high-temperature and high-pressure water in a micro-autoclave.

Compared with passive film formation on stainless steel in aqueous solution at room temperature [30-34], the chromium hydroxide get dehydrated to form Cr_2O_3 in high-temperature and high-pressure , and then improving the corrosion resistance of alloy 690.

The SIMS data yielded a Cr_2O_3 concentration-depth profile, which correlated well with the XPS results. With increasing SMAT duration, the concentrations of Cr_2O_3 increased in the passive film on the surface of treated alloy 690 samples.

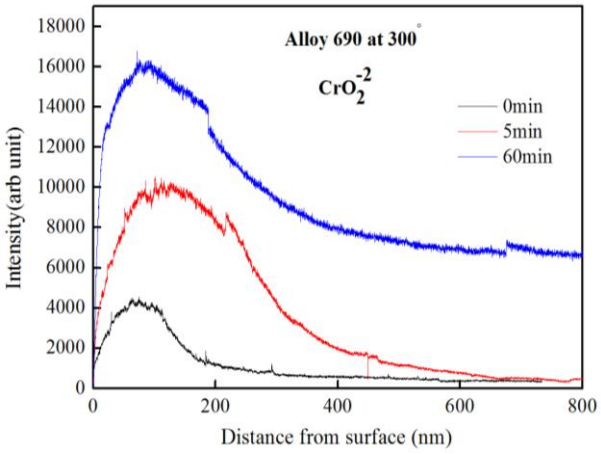

Figure. 6 CrO_2^{-2} concentration-depth profile of Alloy 690 measured using SIMS.

Based on the above observations, we can conclude that treated alloy 690 with smaller grain sizes should exhibit better corrosion resistance in corrosive solutions at high temperatures. The better corrosion resistance demonstrated by the treated samples suggested that SMAT process caused the formation of paths through which Cr can easily diffuse, which allows the rapid formation of a dense protective oxide layer.

4. Conclusions

In this work, we investigated the effect of different SMAT durations on the corrosion properties of alloys used in SG systems.

The XRD and potentiodynamic polarization studies showed that longer SMAT durations reduce grain size and increase microstrain energy in the top surface layer; these effects result in corrosion potential negatively shifting from smaller to larger values and in poor corrosion resistance at the room temperature. After releasing the strain energy in the surface layer by nitriding treatment, recrystallization (i.e., grain growth) occurred in treated

samples, resulting in a lower I_{corr} and improvement of corrosion resistance at room temperature.

Treated alloy 690 exhibited superior corrosion resistance because of the formation of more stable passive films at a high temperature; the breakdown potentials were more positive, and the minimum passive current density decreased with increasing SMAT durations. The XPS results showed that the amount of Cr_2O_3 increased in the passive layer on the surface of alloy 690. Thus, we concluded that the SMAT process caused the formation of paths through which Cr could easily diffuse, thereby allowing the rapid formation of a dense protective oxide layer. The CrO_2^{-2} concentration-depth profile obtained using SIMS was consistent with the XPS and polarization measurements.

Acknowledgements

This research was supported by the National Natural Science Foundation of China (No. 51271157) and a NSERC/Atomic Energy of Canada Ltd (AECL) CRD grant.

Disclosure statement

No potential conflict of interest was reported by the authors.

References

[1] P. Lacombe, B. Baroux, Beranger and G. les aciers inoxydables, les editions de physiques, les Uliscedex A, France, 1990, pp. 663.

[2] W.P. Tong, N.R. Tao, Z.B. Wang, J. Lu, K. Lu, Nitriding iron at lower temperatures, Science 299 (2003) 686-688.

[3] W.L. Li, N.R.Tao, K. Lu, Fabrication of a gradient nano-micro-structured surface layer on bulk copper by means of a surface mechanical grinding treatment, Scr. Mater. 59 (2008) 546-549.

[4] Y.M. Lin, J. Lu, L.P. Wang, T. Xu, Q.J. Xue, Surface nanocrystallization by surface mechanical attrition treatment and its effect on structure and properties of plasma nitrided AISI 321 stainless steel, Acta. Mater. 54 (2006) 5599-5605.

[5] Z.B. Wang, J. Lu, K. Lu, Chromizing behaviors of a low carbon steel processed by means of surface mechanical attrition treatment, Acta. Mater. 53 (2005) 2081-2089.

[6] N.R. Tao, M.L. Sui, J. Lu, K. Lu, Surface nanocrystallization of iron induced by ultrasonic shot peening, Nanostruct. Mater. 11 (1999) 443-440.

[7] G. Liu, J. Lu, K. Lu, Surface nanocrystallization of 316L stainless steel induced by ultrasonic shot peening, Mater. Sci. Eng. A 286 (2000) 91-95.

[8] G. Liu, S.C. Wang, X.F. Lou, J. Lu, K. Lu, Low carbon steel with nanostructured surface layer induced by high-energy shot peening, Scr. Mater. 44 (2001) 1791-1795.

[9] N.R. Tao, Z.B. Wang, W.P. Tong, M.L. Sui, J. Lu, K. Lu, An investigation of surface nanocrystallization mechanism in Fe induced by surface mechanical attrition treatment, Acta. Mater. 50 (2002) 4603-4616.

[10] X. Wu, N. Tao, Y. Hong, B. Xu, J. Lu, K. Lu, Microstructure and evolution of mechanically-induced ultrafine grain in surface layer of AL-alloy subjected to USSP, Acta. Mater. 50 (2002) 2075-2084.

[11] Y. Lin, J. Lu, L. Wang, T. Xu, Q. Xue, Surface nanocrystallization by surface mechanical attrition treatment and its effect on structure and properties of plasma nitrided AISI 321 stainless steel, Acta. Mater. 54 (2006) 5599-5605.

[12] H.W. Zhang, Z.K. Hei, G. Liu, J. Lu, K. Lu, Formation of nanostructured surface layer on AISI 304 stainless steel by means of surface mechanical attrition treatment, Acta. Mater. 51 (2003) 1871-1881.

[13] A.Y. Chen, J.B. Zhang, H.W. Song, J. Lu, Thermal-induced inverse γ/α' phase transformation in surface nanocrystallization layer of 304 stainless steel, Surf. Coat.Technol. 201 (2007) 7462-7466.

[14] Y. Sun, R. Bailey, Improvement in tribocorrosion behavior of 304 stainless steel by surface mechanical attrition treatment, Surf. Coat. Technol. 253 (2014) 284-291.

[15] B. Arifvianto, S.M. Mahardika, Effects of surface mechanical attrition treatment (SMAT) on a rough surface of AISI 316L stainless steel, Appl.Surf. Sci. 258 (2012) 4538-4543.

[16] G. Salvago, G. Fumagalli, D. Sinigaglia, Corros. Sci. 23 (1983) 515–523.

[17] F. Carrette, M.C. Lafont, G. Chatainier, L. Guinard, B. Pieraggi, Analysis and TEM examination of corrosion scales grown on Alloy 690 exposed to pressurized water at 325 °C, Surf. Interface Anal. 34 (2002) 135-138.

[18] A. Machet, A. Galtayries, P. Marcus, P. Combrade, P. Jolivet, P. Scott, XPS study of oxides formed on nickel-base alloys in high-temperature and high-pressure water, Surf. Interface Anal. 34 (2002) 197-200.

[19] S.E. Ziemniak, M. Hanson, Corrosion behavior of NiCrMo Alloy 625 in high temperature, hydrogenated water, Corros. Sci. 45 (2003) 1595-1618.

[20] S.E. Ziemniak, M. Hanson, Corrosion behavior of NiCrFe Alloy 600 in high temperature, hydrogenated water, Corros. Sci. 48 (2006) 498-521.

[21] M. Sennour, L. Marchetti, F. Martin, S. Perrin, R. Molins, M. Pijolat, A detailed TEM and SEM study of Ni-base alloys oxide scales formed in primary conditions of pressurized water reactor, J. Nucl.Mater. 402 (2010) 147-156.

[22] O. Grässel, L. Krüger, G. Frommeyer, L.W. Meyer, High strength Fe–Mn–(Al, Si) TRIP/TWIP steels development — properties — application, Int. J. Plast. 16 (2000) 1391-1409.

[23] S. Yin, D.Y. Li, R. Bouchard, Effects of the strain rate of prior deformation on the wear–corrosion synergy of carbon steel, Wear 263 (2007) 801-807.

[24] V. Maurice, W.P. Yang, P. Marcus, XPS and STM investigation of the passive film formed on Cr(110) single-crystal surfaces, J. Electrochem. Soc. 141 (1994) 3016-3027.

[25] A.M. Salvi, J.E. Castle, J.F. Watts, E. Desimoni, Peak fitting of the chromium 2p XPS spectrum, Appl. Surf. Sci. 90 (1995) 333-341.

[26] J.E. Castle, C.R. Clayton, Passivity of metals, in: R.P. Frankenthal, J. Kruger (Eds.), The Electrochemical Society, Princeton, NJ, USA, 1978, pp. 714.

[27] N.S. McIntyre, D.G. Zetaruk, D. Owen, XPS study of the initial growth of oxide films on Inconel 600 alloy, Appl. Surf. Sci. 2 (1978) 55-73.

[28] D. Zuili, V. Maurice, P. Marcus, In situ scanning tunneling microscopy study of the structure of the hydroxylated anodic oxide film formed on Cr(110) single-crystal surfaces, J. Phys. Chem. B 103 (1999) 7896-7905

[29] P. Marcus, J.M. Grimal, The anodic dissolution and passivation of NiCrFe alloys studied by ESCA, Corros. Sci. 33 (1992) 805-814.

[30] M.P. Ryan, R.C. Newman, G.E. Thompson, A scanning tunnelling microscopy study of structure and structural relaxation in passive oxide films on Fe-Cr alloys, Philosophical.Mag. B 70 (1994) 241-251.

[31] M.P. Ryan, R.C. Newman, G.E. Thompson, Atomically resolved STM of oxide film structures on Fe-Cr alloys during passivation in sulfuric acid solution, J. Electrochem. Soc. 141 (1994) L164-L165.

[32] V. Maurice, W. Yang, P. Marcus, XPS and STM study of passive films formed on Fe-22Cr(110) single-crystal surfaces, J. Electrochem. Soc. 143 (1996) 1182-1200.

[33] H. Nanjo, R.C. Newman, N. Sanada, Atomic images of 304SS surface after electrochemical treatments, Appl. Surf. Sci. 121 (1997) 253-256.

[34] V. Maurice, W. Yang, P. Marcus, X-ray photoelectron spectroscopy and scanning tunneling microscopy study of passive films formed on (100) Fe-18Cr-13Ni single-crystal surfaces, J. Electrochem. Soc. 145 (1998) 909-920.

Table

Table 1. Chemical composition of the experimental materials (wt. %)

Type	C max	Mn max	P max	C max	Si max	Cr	Ni	Mo	Fe
304	0.08	2.0	0.045	0.03	1.0	18-20	8-12	--	Bal
316L	0.08	2.0	0.045	0.03	1.0	16-18	10-14	2-3	Bal
690	0.03	0.18	--	--	0.03	29.4	Bal	0.01	9.2

Table 2. Average grain size and mean microstrain in the surface layer of the 316L samples derived from XRD analysis

SMAT processing duration (min)	*D* (nm)	ε_2 (%)
5	21	0.182
15	17	0.201
30	13	0.228
60	9	0.263

Figure 1. XRD profiles of (a) the untreated and SMATed 316 samples and (b) the untreated and SMATed 690 samples with different durations

Figure. 2 Potentiostatic polarization curves of (a) 316L, and (b) 690 with different SMAT durations

Figure.3 SMATed 316L with nitriding treatment after SMAT.

Figure 4. Polarization curves of alloy 690 at 300 $^{\circ}$C after different SMAT durations.

Figure. 5. Cr $2p_{3/2}$ core-level spectra of alloys 690 after SMATed for 0,5 and 60 minutes respectively exposed to high-temperature and high-pressure water in a micro-autoclave.

Figure. 6 CrO_2 concentration-depth profile of Alloy 690 measured using SIMS.

Graphical Abstract

Click here to download high resolution image